Sediment trap experiments in the deep North Atlantic: isotopic and elemental fluxes

by Peter G. Brewer,[1] Yoshiyuki Nozaki,[1,2] Derek W. Spencer[1] and Alan P. Fleer[1]

ABSTRACT

We have carried out sediment trap experiments at sites in the Sargasso Sea (S_2) and in the Atlantic off Barbados (E) to determine the mass flux and chemical composition of material sinking to the sea floor. At the S_2 site, the mass flux increases with depth from 280-740 $\mu g\ cm^{-2}\ yr^{-1}$; at the E site the flux is constant at 1800 $\mu g\ cm^{-2}\ yr^{-1}$. Chemical analyses show that K, Ti, Al, La, V, Co and ^{232}Th are derived largely from terrigenous materials whereas Ca, Sr, Mg, Si, Ba, ^{226}Ra, U and I are carried by biogenic particles. The reactive elements Mn, Cu, Fe, Sc and $^{230,234}Th$, show increasing ratios to Al with depth due to scavenging from the water column. We calculate a mean particle settling velocity of 21 m day^{-1}, and scavenging residence times ranging from 22 years for Th to 500 years for Cu. The flux of aluminosilicates increases with depth, and this cannot be attributed to changes in trap efficiency. Thus horizontal transport of material must be invoked.

1. Introduction

The study of the flux of particulate material to the ocean floor has received considerable attention in the past few years. Important questions relating to the food supply for benthonic organisms, the construction of the sedimentary record, and dissolution and adsorptive processes occurring in the water column remain to be answered, and are best addressed by direct observations of the particulate flux. Various techniques have been used to obtain particulate matter samples including water collection and shipboard filtration (Brewer *et al.*, 1976), *in situ* filtration from electrically powered pumps (Krishnaswami and Sarin, 1976a; Bishop *et al.*, 1977) and sediment traps. Although sediment trap experiments (Berger and Soutar, 1967; Wiebe *et al.*, 1976; Hinga *et al.*, 1979; Deuser and Ross, 1980) do yield a direct observation of flux, and permit detailed analysis of discrete particle fractions such as fecal pellets, planktonic tests, anthropogenic particles (Honjo, 1978, 1980), they are rendered complex by ambiguities concerning trap efficiency (Hargrave and Burns, 1979; Gardner, 1980a) differential settling rates and resuspension of bottom sedi-

1. Woods Hole Oceanographic Institution, Woods Hole, Massachusetts 02543.
2. Present address: Ocean Research Institute, Tokyo University, 1-15-1, Minamidai, Nakano-Ku, Tokyo 164, Japan.

ments (Spencer *et al.*, 1978; Gardner, 1980b). Floating sediment trap results from the upper 1000 m of the North Pacific have recently been reported by Knauer *et al.* (1979). We have recently conducted a series of deep sea moored sediment trap experiments and report here results obtained from experiments in the Sargasso Sea and in the Atlantic off Barbados. The taxonomic and mineralogic data for these samples is given by Honjo (1980); elemental and isotopic data are described here.

2. Methods

a. Field work and hydrographic data. The first experiment was a repeat of the experiment reported by Spencer *et al.* (1978) and Honjo (1978) at a Sargasso Sea site (31°34′ N, 55°03′W), here referred to as S_2. The mooring was deployed and recovered from the R.V. *Oceanus* from July-October, 1977 for a period of 110 days. The second experiment was carried out at a new site in the tropical North Atlantic approximately 300 miles east of Barbados on the Demerara Abyssal Plain at 13°05′N, 54°00′W. Deployment at this site, designated *E*, was from R.V. *Oceanus* and recovery from R.V. *Atlantis II*, covering a 98-day period from November, 1977 to February, 1978.

The traps were similar to those used previously (Honjo, 1978; Spencer *et al.*, 1978), and described in detail by Honjo and Connell (1979). They basically consist of a P.V.C. cone of 60° angle, presenting a 1.5 m² opening fitted with a 25 cm honeycomb grid to reduce turbulent washout. Particulate material falling into the cone was collected in a lucite sample cup, closed at the end of the deployment period by a timer-controlled spring-loaded door. The cup was fitted with a sodium chloride/sodium azide pellet which bled continuously into the sample cup to retard bacterial spoilage of the trapped sample. The traps were mounted singly in a structural aluminum tubing frame and deployed on a mooring with subsurface flotation, balanced by the placing of glass flotation balls on each trap frame and along the wire. Sketches of the moorings used are shown in Figure 1.

The hydrographic conditions at the *S* site have been described previously by Spencer *et al.* (1978). In particular the existence of a distinct nepheloid layer extending more than 500 m above the bottom at this site had a profound influence on the first experiment, contributing more than half of the observed mass flux to a trap set at 5367 m. For the second experiment at this site traps were set at 372, 976, 3964 and 5206 meters. The lower three traps operated perfectly, though the bottom sample appeared to be contaminated by corroded aluminum metal from a defect in the sliding door coating, and for this reason, chemical data for this sample are not reported here.

The *E* site is situated approximately mid-way between GEOSECS Stations 36 and 37 at a water depth of 5288 m. The water column is characterized by a weak oxygen minimum between 200 and 400 meters. A nephelometer lowering showed

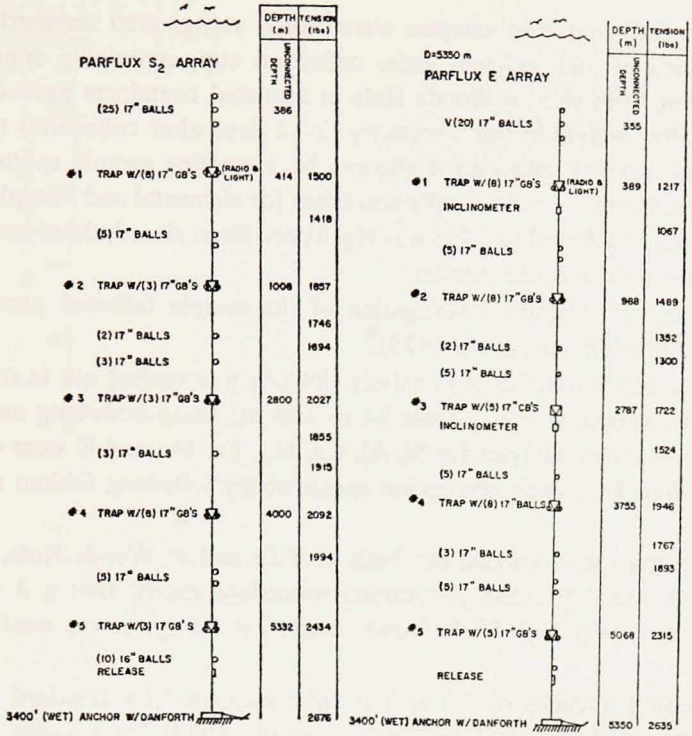

Figure 1. Sketches of the moorings at the *E* and S_2 sites.

no significant increase in light scattering near bottom, though a weak increase was observed at GEOSECS Station 37 (GEOSECS Leg Reports, Leg 4). Particulate matter samples were collected by means of 30 *l* Niskin bottles and filtered through pre-weighed 0.6 μm pore size. Nuclepore filters. Filters were distilled water rinsed, stored and weighed ashore. The results (Table 1) reveal mid-water concentrations close to 3 μg/kg increasing to 10 μg/kg near bottom.

Table 1. Suspended particulate matter concentrations at the PARFLUX *E* site (13°05′N, 54°00′W).

Depth (m)	Concentration (μg/kg)	Depth (m)	Concentration (μg/kg)
1	17	1994	2
52	12	2415	—
104	10	2995	1
203	7	3496	3
402	4	3997	5
701	6	4495	5
1000	3	5019	6
1488	3	5256	10

b. Analytical. Sediment trap samples were stored refrigerated onboard ship and were transported in their original lucite collection cup, containing approximately 2 *l* of sea water, from ship to Woods Hole in insulated containers packed with ice. Immediately after arrival in the laboratory (2-12 days after collection) the sample from each cup was wet split into 4 aliquots by a rotating sample splitter (Honjo, 1978). One quarter of the total sample was taken for elemental and isotopic analyses. The sample was transferred to a 0.5 μm Nuclepore filter, rinsed, dried and weighed, then homogenized in an agate mortar.

The chemical and isotopic investigation of the sample followed previously described procedures (Spencer *et al.*, 1978).

Instrumental neutron activation analysis (INAA) was carried out in triplicate on fractions of the sample weighing from 94 to 430 μg, using both long and short irradiations. In addition, analyses for Si, Al, Ca, Mg, Fe, Mn and K were carried out on 0.2 g fractions by atomic absorption spectroscopy following lithium metaborate fusion.

Isotopic analyses were carried out both at Yale and at Woods Hole. ^{234}Th was measured by a non-destructive β-counting procedure except that a 2 π gas flow counter with relatively high background counts ($\sim$ 10 cpm) was used at Woods Hole.

The α-emitting nuclides of Th and U were measured by standard procedures (Krishnaswami and Sarin, 1976b; Turekian *et al.*, 1973) for samples totally dissolved with HF-HNO_3 in the presence of ^{234}Th and ^{236}U (Woods Hole) or ^{232}U (Yale) spikes. ^{231}Pa was analyzed by the procedure of Krishnaswami (personal communication) by using ^{233}Pa as a yield tracer. Approximately 50 mg was dissolved with HF-HNO_3 in the presence of ^{233}Pa spike. 5 ml of concentrated $HClO_4$ was added to the sample and then evaporated to complete dryness. This procedure was repeated twice. The sample was then dissolved in 25 ml of 8 N HNO_3 and passed through an ion-exchange column (Dowex 1×8, 100-200 mesh). The adsorbed U, Th, and Pa isotopes were eluted with 50 ml of dilute HCl solution ($\sim$ 0.1 M) and the eluate was evaporated to dryness. The isotopes were then dissolved in 5 ml of 6 N HCl solution. Pa was extracted into 0.4 M TTA in benzene and deposited on a stainless steel disc. The α-counting systems are identical to those described previously. ^{226}Ra was measured at Yale by the ^{222}Rn emanation method (Turekian *et al.*, 1973).

3. Results

Basic data on the sediment trap deployments and on the mass of material recovered is presented in Table 2. The elemental composition of the samples is given in Table 3, together with an indication of the analytical method used. Where two techniques were used, both sets of data are presented. In most cases the agreement

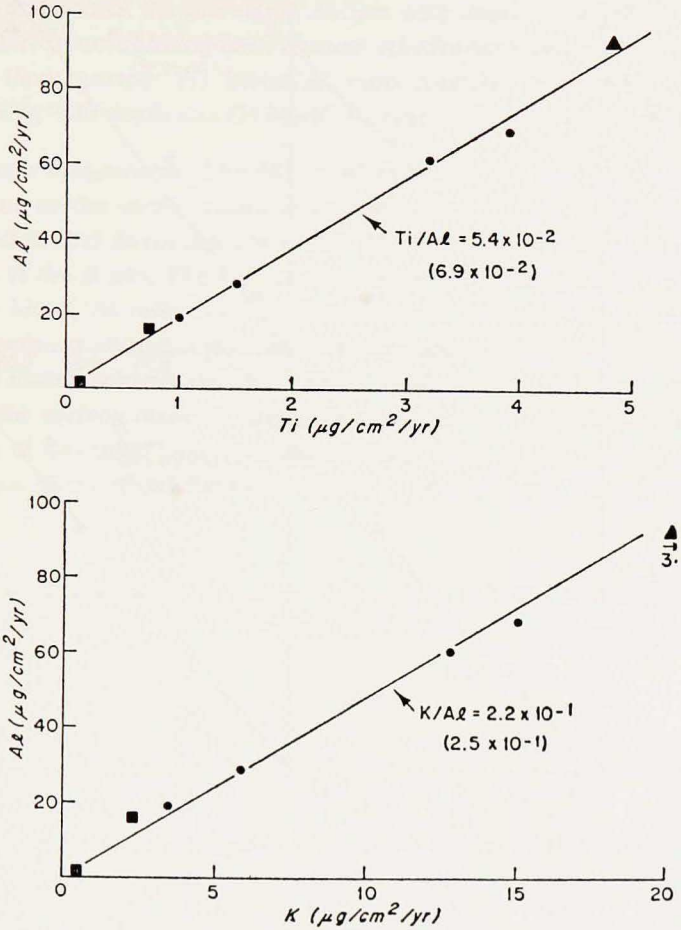

Figure 2. Correlation diagram between Ti and Al (above) and between K and Al (below). Circles, triangles and squares represent data at the *E* site, S_1 site and S_2 site, respectively in this and subsequent figures.

is remarkably good considering the small sample size available. The greatest discrepancy occurs in the determination of Mg, where poor counting statistics lead us to prefer the atomic absorption data. The calculated elemental fluxes are given in Table 4.

The radionuclide data are given in Table 5. Since there is no systematic difference in results obtained in two laboratories, the mean values are listed with either standard deviation or counting error, whichever is greater.

The results for ^{234}Th, ^{210}Po and ^{228}Th in Table 5 are decay corrected as described by in our earlier work.

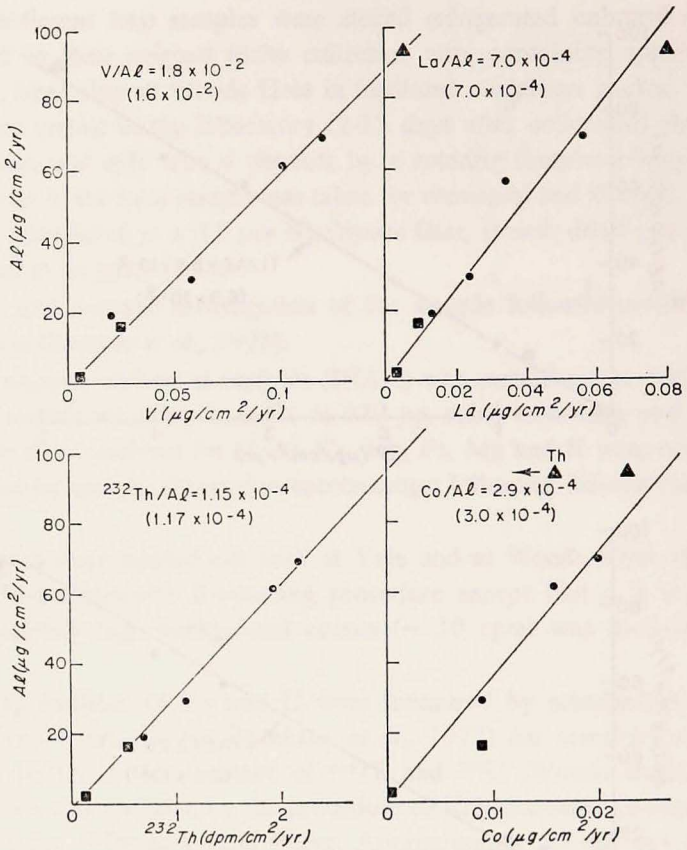

Figure 3. Correlation diagrams for V, La, ^{232}Th, Co versus Al.

4. Discussion

Based upon the data presented here, it is possible to deduce the factors affecting the chemical composition of the sample. Since Al increases both in concentration and flux with depth, we will first proceed by normalizing each element relative to

Table 2. Sediment trap deployment and total flux results.

	S_2 (31°32.5′N 55°55.4′W) 7/77-10/77 (110 Days)		E (13°30.2′N 54°00.1′W) 11/77-2/78 (98 Days)			
Depth (m)	976 m	3694 m	389 m	988 m	3755 m	5086 m
Dry weight* (g)	1.26	3.36	7.60	6.48	7.88	7.28
Flux (μg cm^{-2} yr^{-1})	278	743	1887	1609	1956	1807

* Results calculated from weighing 1/2 of the split sample.

Al. The observation of the increasing Al flux with depth is surprising, and will be discussed later. In normalizing each element relative to Al we find that the elements divide into three groups: (1) Metal/Al ratio constant with depth; (2) Metal/Al ratio decreasing with depth and (3) Metal/Al ratio increasing with depth.

a. Terrigenous components. The Metal/Al ratios for K, Ti, La, V, Co and ^{232}Th are very close to the mean crustal abundance ratios (Taylor, 1964). In Figures 2 and 3 the calculated fluxes are compared. The correlation lines were drawn based on the data at the *E* site. The fact that all the lines go through zero with the slope indicating a Metal/Al ratio close to that of crustal abundances suggests that these elements are almost entirely incorporated in terrigenous materials.

Fe is well correlated with Al with a Fe:Al ratio of 1:2. The source of terrigenous material at the surface ocean is largely from atmospheric deposition. The chemical composition of this input into the tropical North Atlantic has recently been investigated by Buat-Menard and Chesselet (1979). The Fe:Al ratio in this surface ocean

Table 3. Elemental composition of sediment trap samples determined by instrumental neutron activation analysis and by atomic absorption spectroscopy.

		Trap depths					
		E site				S_2 site	
Analysis	Element	389 m	988 m	3755 m	5086 m	976 m	3694 m
AA	Si (%)	8.62	11.0	13.6	14.9	5.52	7.05
AA	Al (%)	0.76	1.31	2.89	3.64	0.80	2.18
INAA		1.03	1.76	3.11	3.79	0.82	2.14
AA	Ca (%)	21.7	20.5	20.9	18.3	24.7	26.4
INAA		21.2	21.8	21.2	19.06	24.7	24.9
AA	Mg (%)	0.61	0.57	0.77	0.84	0.50	0.62
INAA		0.706	0.80	1.15	1.45	0.60	0.77
AA	Mn (ppm)	56	78	330	460	46	780
INAA		34	65	315	464	61	756
AA	Fe (%)	0.34	0.81	1.58	1.91	0.50	0.75
INAA		0.18	0.60	1.30	1.84	0.35	0.75
AA	K (%)	0.18	0.35	0.65	0.84	0.26	0.31
INAA	Ba (ppm)		670	658	511	689	631
INAA	Ti (ppm)	537	927	1614	2176	566	918
INAA	Sr (ppm)	1354	1514	1581	1250	1755	1790
INAA	Cu (ppm)		29	80	129	203	279
INAA	V (ppm)	11	36	52	66	17	34
INAA	I (ppm)	219	169	132	135	311	203
INAA	La (ppm)	6.8	14.8	17.8	27.9	10	12
INAA	Sc (ppm)	0.92	2.51	4.92	6.62	1.05	1.85
INAA	Zn (ppm)	600	440	340	470	218	345
INAA	Co (ppm)		2.5	7.9	11.2	8.0	13.1

particulate fraction is 3:1. The six-fold decrease in this ratio, observed in our samples, could represent stripping of a reactive iron phase from the aluminosilicate material by marine organisms.

The good correlation between ^{232}Th and Al (Fig. 3) suggests that ^{232}Th is contained almost entirely in clay phases, in which the daughters of ^{232}Th should be near equilibrium with the parent. This then provides a basis for estimating the unsupported fraction of the Th series daughter nuclides in the trapped material.

b. The biogeneous components. The second group of elements, Ca, Sr, Mg, Si, Ba, ^{226}Ra, U and I, is characterized by Metal/Al ratio decreasing with depth. These elements are all known to be incorporated to some extent in biogenic particles, such as carbonates, opal and organic matter. Since the terrigenous components are well expressed by their relative crustal abundances, it is possible to calculate the biogenic components by making certain assumptions.

If we assume that Ca, Sr, and Mg are all present solely in carbonates and clay mineral phases, then, calculating in units of flux, the $CaCO_3$ fraction can be calculated by:

Table 4. Elemental fluxes in $\mu g\ cm^{-2}$ calculated from sediment trap data.

		Trap depths					
		E site				S_2 site	
Analysis	Element	389 m	988 m	3755 m	5086 m	976 m	3694 m
AA	Si	163	177	266	269	15.3	52.4
AA	Al	14.3	21.1	56.5	65.8	2.22	16.2
INAA		19.4	28.3	60.8	68.5	2.28	15.9
AA	Ca	410	330	409	331	68.7	196
INAA		400	351	415	344	68.7	185
AA	Mg	11.5	9.17	15.1	15.2	1.39	4.61
INAA		13.3	12.9	22.5	26.2	1.67	5.72
AA	Mn ($\times 10^4$)	1057	1255	6455	8312	128	5795
INAA		642	1046	6161	8384	170	5617
AA	Fe	6.42	13.0	30.9	34.5	1.39	5.57
INAA		3.40	9.65	25.4	33.2	0.97	5.57
AA	K	3.40	5.63	12.7	15.2	0.72	2.30
INAA	Ba ($\times 10^4$)		10780	12870	9234	1915	4688
INAA	Ti ($\times 10^4$)	10130	14920	31570	39320	1573	6821
INAA	Sr ($\times 10^4$)	25550	24360	30920	22590	4879	13300
INAA	Cu ($\times 10^4$)		467	1565	2331	564	2073
INAA	V ($\times 10^4$)	208	579	1017	1193	47.3	253
INAA	I ($\times 10^4$)	4132	2719	2582	2439	864	1508
INAA	La ($\times 10^4$)	128	238	348	504	27.8	89.2
INAA	Sc ($\times 10^4$)	17.4	40.4	96.2	120	2.92	13.7
INAA	Zn ($\times 10^4$)	11320	7080	6650	8493	606	2563
INAA	Co ($\times 10^4$)		40.2	154	202	22.2	97.3

$$\underset{(\%)}{CaCO_3} = \{(Ca + Mg + Sr)_{meas} - \left(\frac{Ca + Mg + Sr}{Al}\right)_{crust} \times Al_{meas}\} \times \frac{100}{40} \times \frac{100}{\Sigma F} \quad (1)$$

where Mg and Sr are stoichiometrically converted to Ca as an approximation and ΣF is the total material flux. The water content is taken to be zero. Here the fraction of Ca, Mg and Sr in clay phases is estimated by using crustal abundances. This assumption may not be exactly correct because the Ca concentration varies widely in crustal materials. However, the fraction is at most 10% of the total Ca flux, so that deviations of the Ca/Al ratio from the assumed values will not cause serious error. Similarly, by assuming that all the Si exists solely in opaline silica and clay phases, the fraction of biogenic silica is given by:

$$SiO_2\,(\%) = \{Si_{meas} - \left(\frac{Si}{Al}\right)_{crust} \times Al_{meas}\} \times \frac{60}{28} \times \frac{100}{\Sigma F} \quad (2)$$

In this case, the Si fraction in clay particles is quite large. Fortunately, however, the Si content of crustal materials is nearly constant within ± 10%, so the calculation is reasonably reliable.

Table 5. Radionuclide concentrations (dpm/g).

	PARFLUX *E* site				PARFLUX *S* site	
Trap Depth	389 m	988 m	3755 m	5086 m	1000 m	4000 m
Nuclide						
^{234}Th	4320 ± 343	3589 ± 79	3251 ± 20	3411 ± 326	9044 ± 990	5458 ± 1284
^{228}Th	13.5 ± 1.9	12.9 ± 2.6	12.5 ± 1.1	18.4 ± 2.8	61.1 ± 1.5	50.5 ± 9.8
^{230}Th	0.53 ± 0.8	1.45 ± 0.07	4.21 ± 0.29	5.37 ± 0.80	2.03 ± 0.37	8.04 ± 1.14
^{232}Th	0.37 ± 0.13	0.69 ± 0.08	0.99 ± 0.11	1.20 ± 0.22	0.57 ± 0.11	0.77 ± 0.12
^{210}Pb	95 ± 6	148 ± 14	331 ± 41	376 ± 38	219 ± 9	476 ± 39
^{210}Po	122 ± 5	104 ± 12	499 ± 15	667 ± 20	281 ± 11	876 ± 10
^{226}Ra	3.47 ± 0.10	2.57 ± 0.23	1.87 ± 0.48	1.60 ± 0.85	6.95 ± 0.40	7.06 ± 0.40
^{238}U	1.2 ± 0.17	1.0 ± .15	1.0 ± 0.13	1.1 ± 0.15	2.27 ± 0.23	1.28 ± 0.10
^{231}Pa		0.093 ± 0.007	0.25 ± 0.04	0.27 ± 0.02		

The remainder of the material we consider to be largely organic matter, which is given by

$$\text{Organic Matter } (\%) = 100 - CaCO_3 - SiO_2 - \text{Clay} \qquad (3)$$

where the clay phase is calculated by assuming an Al content of 8.23% (Taylor, 1964). The calculated results are given in Table 6, together with the measured values of $CaCO_3$ and organic matter (Honjo, personal communication). The estimated $CaCO_3$ is consistently lower than the values measured by Honjo, but the decreasing trend with depth is consistent. For the organic matter, the agreement between the calculated values and measured values is remarkable. It is clear that the clay fraction increases with depth, while all biogenic fractions decrease with depth. Honjo (1978, 1980) demonstrated that most biogenic particles are transported very rapidly as fecal pellets. The organic matter content of the bottom trap samples (10%) is very high compared to that of deep sea sediments. This suggests that a significant fraction of organic matter derived from the surface must be consumed at the water-sediment interface. The observed mole ratios of the fluxes of carbonate and organic carbon are approximately 3:2. If this represents the delivery ratio to the sediments at this site, then respiratory production of CO_2 from metabolism of the organic carbon could be responsible for dissolving ~ 67% of the carbonate flux at the water-sediment interface.

It is interesting that certain minor elements in the second group can be related to specific biogenic components. Iodine is best correlated with organic matter with a slope of 1300 ppm (Fig. 4) which is approximately sixfold higher than the results of Wong *et al.* (1976), who reported a slope of 200 ppm for the fine particulate fraction. The total concentration of U is nearly constant in samples collected at the *E* Site, which does not correlate with any one of the single components. The fact that the U concentrations, ranging between 1 and 2.3 dpm/g, are close to the crustal abundance (~ 2 dpm/g) indicates that the other fractions also have a similar U concentration. By assuming a uniform distribution of U between clay and biogenic

Table 6. The estimated particle composition of the trapped material ( ).

		Clay	$CaCO_3$		Opal	Organic Matter	
PARFLUX							
E	398 m	12.1	53.5	(62.7)	11.1	23.3	(19.7)
	998 m	21.0	51.1	(55.1)	10.0	17.9	(17.5)
	3755 m	37.5	48.5	(56.3)	6.5	7.5	(10.3)
	5086 m	45.9	41.2	(49.2)	4.4	8.5	(10.4)
PARFLUX							
S_2	1000 m	9.4	65.6	(43.7)	6.5	18.2	(17.6)
	4000 m	25.9	62.6	(68.0)	0	11.5	(10.0)

(Numbers in parentheses are the values measured by Honjo (1979)).

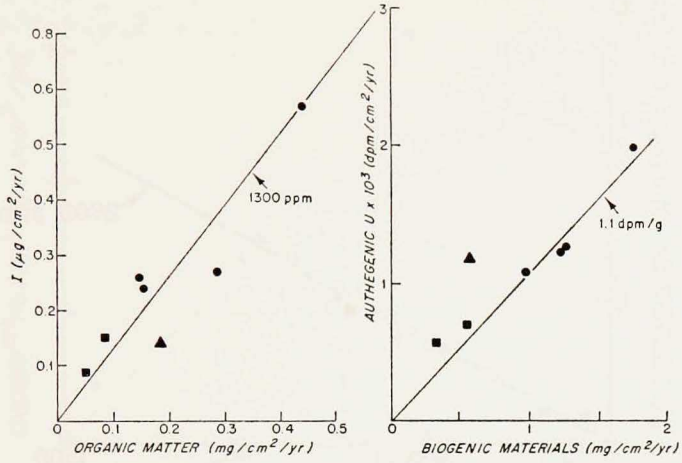

Figure 4. Correlation diagram between I and calculated organic matter (left) and between authigenic U and total biogenic materials (right). Authigenic U was calculated by assuming a uniform uranium concentration of 1.1 dpm/g in the trapped material.

particles, the biogenic U fraction may be calculated. This is plotted against total trapped biogenic material in Figure 4, which shows a linear relationship with a slope of 1.1 dpm/g. The biogenic U fraction is probably taken up from sea water independent of its daughter nuclides, whereas the clay U fraction must be in close equilibrium with its daughters. This provides a basis for calculating the excess U series daughter nuclides unsupported by ^{238}U. The clay corrected Sr versus $CaCO_3$ plot (Fig. 5) gives a slope of 2800 ppm which is ~ 3 times higher than the average Sr content of deep-sea calcareous tests (Turekian, 1965). Honjo (1979) has examined these samples for acantharia tests and found none in the trapped material, though these organisms are common in filtered samples from the water column. ^{226}Ra is best correlated with biogenic SiO_2 with a slope of 26 dpm/g SiO_2 (Fig. 6) which is consistent with the estimate of 28 dpm/g SiO_2 calculated from GEOSECS water column data (Broecker *et al.*, 1976).

The barium fluxes reported here are not well correlated with the biogenic opal or carbonate fluxes, in spite of the apparent relationship between dissolved Ba and dissolved $Si(OH)_4$ (Chan *et al.*, 1977). Dehairs *et al.* (1980) have recently examined the flux of particulate Ba in detail. They conclude that discrete particles of barite ($BaSO_4$) are responsible for much of the barium flux, and that these have a biogenic origin. They estimate the total particulate flux of Ba in the North Atlantic to be approximately 1.3 $\mu g\ cm^{-2}\ yr^{-1}$. Our data are in good agreement with their concepts.

c. The scavenged elements. The third group of elements, Mn, Cu, Fe, Sc and ^{230}Th are characterized by an increase in the Metal/Al ratio with depth, as shown in

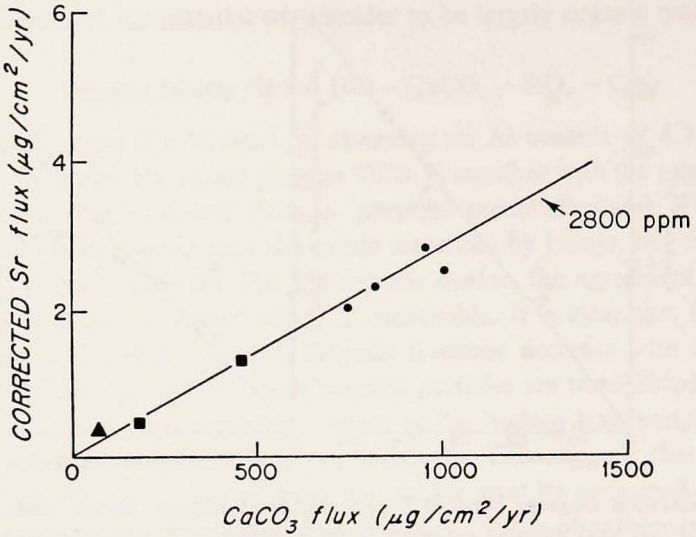

Figure 5. Correlation diagram between clay corrected Sr and calculated $CaCO_3$ flux. Symbols are the same as Figure 2.

Figure 7. Since all the biogenic particles decrease with depth (Table 6), the increase in the Metal/Al ratio cannot be explained by the contribution of biogenic components. The metals in this group are known to be highly surface active in sea water, as indicated by their short oceanic residence times (e.g., Brewer, 1975), and are expected to be scavenged by settling particles from sea water. The scavenging of the reactive elements from sea water is shown even more strikingly in the radionuclide data (Table 5). The concentrations of the short-lived nuclides ^{234}Th, ^{228}Th, ^{210}Pb and ^{210}Po are extremely high compared to those of surface sediments. The short-lived ^{234}Th (half-life, 24 days) concentrations are nearly constant at the *E* site, although particle composition varies significantly with depth. This is to be expected if scavenging from seawater is approximately balanced by radioactive decay in particulate ^{234}Th, and if there is no significant difference in scavenging properties between different particle fractions. Based upon these observations, it is of interest to examine whether our radionuclide and reactive metal data are consistent with a vertical scavenging and settling model (Craig, 1974; Spencer *et al.*, 1978; Brewer and Hao, 1979).

5. Application of a scavenging and settling model

We have previously applied a vertical scavenging and settling model to a set of radionuclide data obtained from a sediment trap pair at 5367 meters depth in the Sargasso Sea and derived two possible solutions for the mean settling velocity and scavenging rate of Th. The application of this model to a depth series of data should

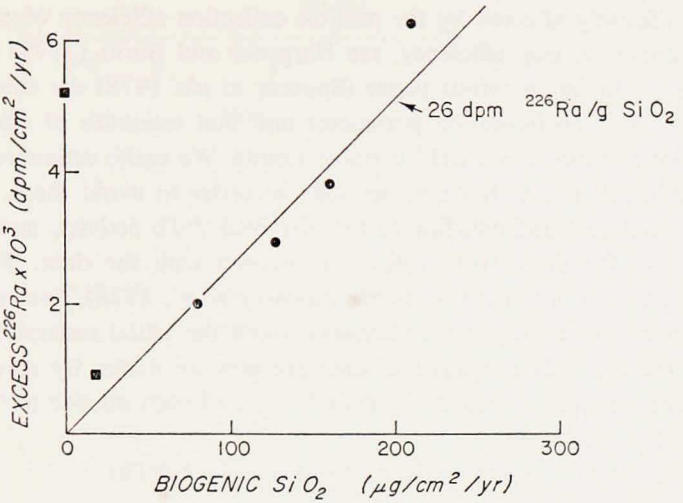

Figure 6. Correlation diagram between excess ^{226}Ra and calculated biogenic SiO_2. Excess ^{226}Ra was calculated by subtracting the uranium-supported fraction in clay phases.

provide a unique solution for these parameters. Although simple vertical models for dissolved species are open to substantial criticism for neglecting the very large horizontal terms, for the rapidly sinking particles observed here the assumptions are quite good and the only data set available to us is purely one-dimensional.

Following the terminology of Spencer *et al.* (1978), the steady state distribution of the particulate radionuclides is given by:

$$S\frac{\partial \chi}{\partial Z} + \psi C + \lambda_p \chi_p - \lambda \chi = 0 \qquad (4)$$

S is the mean settling velocity of the particles (cm sec^{-1}), ψ is the first order scavenging rate constant (sec^{-1}), λ is the decay constant, and the concentrations of the radionuclides (atoms kg^{-1} sea water) in particulate phases are denoted by χ and in solution by C. The $\lambda_p \chi_p$ term, the production rate of the daughter nuclide from its parent nuclides within the particles, was added to the equation (1) in Spencer *et al.* (1978). This term is significant only for ^{210}Po, because the particulate material contains a comparable amount of its parent nuclide, ^{210}Pb. The scavenging rate, ψC is deduced from the measured distribution of the radionuclide concentration, or the distribution of its parent nuclide, in the water column.

A straightforward application of the model is to fit the solution of equation (4) to the suspended particulate radionuclide concentration (dpm/kg). However, this quantity is not known exactly; because the particles analyzed here, and responsible for the flux, are probably biased toward larger sizes they may not be representatively sampled by traditional Niskin bottle methods. The measured radionuclide fluxes

are also significantly affected by the particle collection efficiency of each trap (for interesting studies of trap efficiency, see Hargrave and Burns (1979) and Gardner (1980a and b). In our previous paper (Spencer *et al.*, 1978) we showed that the trap efficiency was an important parameter and that estimates of efficiency based upon different isotopes could yield variable results. We make estimates of trap efficiency later in this paper, however, initially in order to avoid these problems we have normalized each radionuclide to the observed ^{234}Th activity, and the solution of equation (4) for the activity ratio is compared with the data. Therefore, the trapping efficiency ϵ in our earlier paper (Spencer *et al.*, 1978), does not appear in this calculation. No assumption is necessary about the initial radionuclide fluxes at the upper boundary, since a series of data are now available. By solving equation (4) and rearranging the solutions, the activity ratio of each nuclide to ^{234}Th is given by the following equations:

(a) For the activity ratio of ^{230}Th to ^{234}Th ($A^{230}Th/A^{234}Th$),

$$\frac{A_{^{230}Th}}{A_{^{234}Th}} = \left(\frac{\lambda_{^{234}Th} + \psi_{Th}}{\lambda_{^{230}Th} + \psi_{Th}}\right)\left(\frac{C_1'}{C_1}\right)\left(\frac{1 - \exp\left(-\frac{\lambda_{^{234}Th}}{S} \cdot Z\right)}{1 - \exp\left(-\frac{\lambda_{^{234}Th}}{S} \cdot Z\right)}\right) \quad (5)$$

where C_1'/C_1 is the activity ratio of ^{234}U/^{238}U (1.15).

(b) For ^{228}Th/^{234}Th,

$$\left(\frac{A_{^{228}Th}}{A_{^{234}Th}}\right) = \left(\frac{\psi_{Th} + \lambda_{^{234}Th}}{\psi_{Th} + \lambda_{^{228}Th}}\right)\left(\frac{1}{1 - \exp\left(-\frac{\lambda_{^{234}Th}}{S} \cdot Z\right)}\right)$$

$$\left[\left(\frac{\lambda_{^{228}Th}}{S\alpha - \lambda_{^{228}Th}}\right)\left(\frac{C_2}{C_1}\right)\left(\exp\left(-\frac{\lambda_{^{228}Th}}{S} \cdot Z\right) - \exp(-\alpha Z) + \right.\right.$$

$$\left.\left(\frac{\lambda_{^{228}Th}}{S\beta + \lambda_{^{228}Th}}\right)\left(\frac{C_3}{C_1}\right)\left(\exp\{\beta(Z - Z_b)\} - \exp\left\{-\left(\frac{\lambda_{^{228}Th}}{S} \cdot Z + \beta Z_b\right)\right\}\right)\right. \quad (6)$$

$$\left.\left. + \frac{C_4}{C_1} 1 - \exp\left(-\frac{\lambda_{^{228}Th}}{S} \cdot Z\right)\right)\right]$$

where, $\lambda_{^{228}Ra} C_{^{228}Ra} = C_2 \exp(-\alpha Z) + C_3 \exp\{\beta(Z - Z_b)\} + C_4$. (7)

(c) For ^{210}Pb/^{234}Th,

$$\frac{A_{^{210}Pb}}{A_{^{234}Th}} = \frac{(\lambda_{^{234}Th} + \psi_{Th})\,Pb}{\psi_{Th}(S\gamma - \lambda_{^{210}Pb})}\left(\frac{C_5}{C_1}\right)\left(\frac{\exp\left(-\frac{\lambda_{Pb}}{S} \cdot Z\right) - \exp(-\gamma Z)}{1 - \exp\left(-\frac{\lambda_{^{234}Th}}{S} \cdot Z\right)}\right) \quad (8)$$

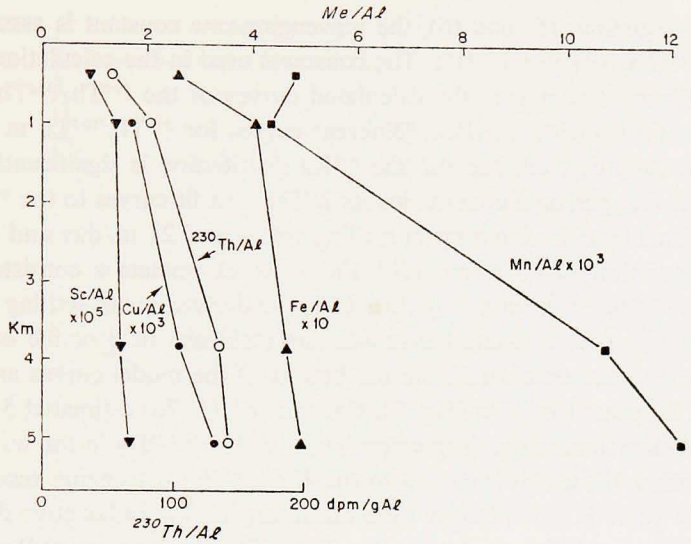

Figure 7. Depth profiles of Metal/Al ratios for Sc, Cu, ^{230}Th, Fe, and Mn at the *E* site.

$$\left(\frac{\psi_{Pb}\,(\lambda_{234_{Th}}+\psi_{Th})}{\psi_{Th}\,\lambda_{210_{Pb}}}\right)\left(\frac{C_6}{C_1}\right)\left(\frac{1-\exp\left(-\frac{\lambda_{210_{Pb}}}{S}\cdot Z\right)}{1-\exp\left(-\frac{\lambda_{234_{Th}}}{S}\cdot Z\right)}\right)$$

where

$$C_{210_{Pb}} = C_5 \exp(-Z) + C_6 \tag{9}$$

(d) For ^{210}Po/^{234}Th,

$$\left(\frac{A_{210_{Po}}}{A_{234_{Th}}}\right) = \left(\frac{\lambda_{210_{Po}}\,\psi_{210_{Po}}\,C_5}{(S\gamma-\lambda_{210_{Pb}})\,(\lambda_{210_{Po}}-\lambda_{210_{Pb}})\,C_1} - \frac{\lambda_{210_{Po}}\,\psi_{Pb}\,C_6}{\lambda_{210_{Pb}}\,(\lambda_{210_{Po}}-\lambda_{210_{Pb}})\,C_1}\right)$$

$$\left(\frac{\exp\left(-\frac{\lambda_{210_{Pb}}}{S}\cdot Z\right)-\exp(-Z)}{1-\exp\left(-\frac{\lambda_{234_{Th}}}{S}\cdot Z\right)}\right) + \left(\frac{\lambda_{210_{Po}}\,\psi_{Po}\,C_5}{(\lambda_{210_{Po}}+\psi_{Po})\,(\lambda_{210_{Po}}-S\gamma)\,C_1}\right. \tag{10}$$

$$\left. - \frac{\lambda_{210_{Po}}\,\psi_{Pb}\,C_5}{(S\gamma-\lambda_{210_{Pb}})\,(\lambda_{210_{Po}}-S\gamma)\,C_1}\right)\left(\frac{\exp(-\gamma Z)-\exp\left(-\frac{\lambda_{210_{Po}}}{S}\cdot Z\right)}{1-\exp\left(-\frac{\lambda_{234_{Th}}}{S}\cdot Z\right)}\right)$$

$$+\left(\frac{\psi_{Pb}\,C_6}{\lambda_{210_{Pb}}\,C_1} \quad \frac{\psi_{Po}\,C_6}{(\lambda_{210_{Po}}+\psi_{Po})\,C_1}\right)\left(\frac{1-\exp\left(-\frac{\lambda_{210_{Po}}}{S}\cdot Z\right)}{1-\exp\left(-\frac{\lambda_{234_{Th}}}{S}\cdot Z\right)}\right)$$

In deriving equations (5) and (6), the scavenging rate constant is assumed to be the same for ^{234}Th, ^{228}Th and ^{230}Th. The constants used in the calculation are listed in Table 7. Figure 8 compares the calculated curves of the ^{228}Th/^{234}Th ratio and the ^{230}Th/^{234}Th ratio with the data. Different curves for ^{228}Th/^{234}Th at the *E* site and the *S* site were derived, because the ^{228}Ra distribution is significantly different at the two sites (Li, personal communication). The best fit curves to the ^{228}Th/^{234}Th data are obtained by choosing a mean settling velocity of 21 m/day and a Th scavenging residence time of 22 years. With the same parameters a consistent fit also results for the ^{230}Th/^{234}Th ratio (Fig. 8). Using the derived mean settling velocity of 21 m/day, we can now estimate the scavenging residence time of the other radionuclides. Those values estimated from the best fit of the model curves are 47 years for ^{210}Pb and 27 years for ^{210}Po (Fig. 9). Bacon *et al.* (1976) estimated 54 years for the ^{210}Pb residence time in the deep water based on ^{210}Pb-^{226}Ra in the water column at Meteor Station 18, which is closest to the *E* site. The scavenging residence time of ^{210}Po of 27 years is much longer than the mean life for radioactive decay, indicating that there should be no deep water disequilibrium between ^{210}Po and ^{210}Pb. This is compatible with the water column results of Bacon *et al.* (1976) and of Turekian and Nozaki (1979). The calculated ^{231}Pa scavenging residence time calculated from three data points at the *E* site is 31 years, which is ~ 15% longer than that of Th.

The concept of elemental scavenging can also be applied to the 'reactive' stable elements (Craig, 1974; Brewer and Hao, 1979) which are characterized by an increasing metal/Al ratio with depth. Since the radioactive decay of ^{230}Th is negligible during particle transit through the water column because of its long half-life (77,000 years), ^{230}Th can be treated as analogous to the stable elements. Therefore, by assuming that the scavenging rate of metals from sea water is proportional to that of ^{230}Th, the following relationship may be derived:

Table 7. Numerical values of various constants used in calculations.

Reference nuclide	Constant	dpm cm^{-3}	Constant	cm^{-1}
^{238}U	C_1	2.45×10^{-3}		
^{234}U	C_1'	2.82×10^{-3}		
	C_2*	1.6×10^{-5}	α*	1.0×10^{-5}
^{228}Ra	C_2**	1.0×10^{-5}	α**	2.5×10^{-6}
	C_3	8×10^{-6}	β	1.8×10^{-5}
	C_4	1×10^{-6}		
^{210}Pb	C_5	9×10^{-5}	γ	4.3×10^{-5}
	C_6	8×10^{-5}		

* values for the *S* site
** values for the *E* site

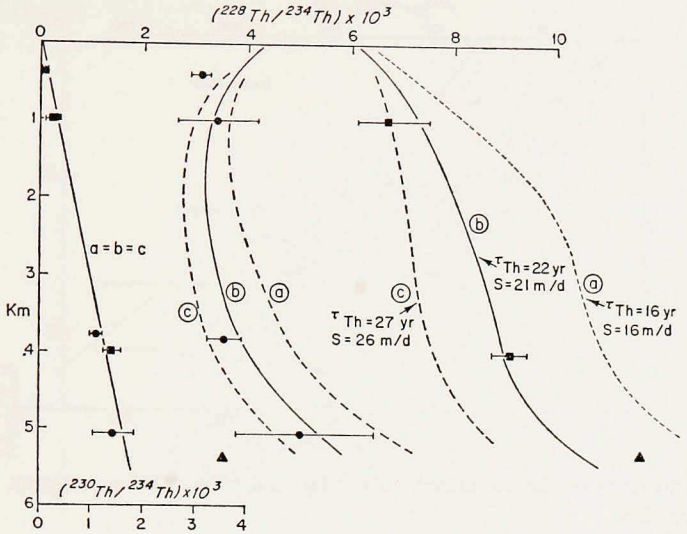

Figure 8. Comparison of the calculated $^{228}Th/^{234}Th$ and $^{230}Th/^{234}Th$ curves with the data. See text for discussion.

$$\left(\frac{Me}{Al}\right)_{measured} = \left(\frac{Me}{Al}\right)_{primary} + \left(\frac{\psi_{Me} C_{Me}}{\psi_{Th} \lambda_{230_{Th}} C_{230_{Th}}}\right)_{scavenged} \times \left(\frac{A_{230_{Th}}}{Al}\right)_{measured} \quad (11)$$

where $(Metal/Al)_{primary}$ is a primary Metal/Al ratio associated with terrigenous particles, $C_{230_{Th}}$ is the dissolved ^{230}Th concentration (atoms/kg) and $A_{230_{Th}}$ is the activity of ^{230}Th in the trapped particles (dpm/g). The amount of ^{230}Th scavenged from sea water is a known quantity, approximated by $\lambda_{230_{Th}} \lambda_{234_U} C_{234_U}$.

In Figure 10, the Metal/Al ratios for Sc, Mn, Fe and Cu are plotted against the $A_{230_{Th}}/Al$ ratio. From the slopes of the curves, the scavenging rate of each element, $\psi_{Me} C_{Me}$, is obtained. By taking the slopes from data at 988 meters and 3755 meters as average ocean values and using the most recent published values for the dissolved concentrations of these metals in seawater, the residence times of each element may be calculated. These results are given in Table 8. The calculated results compare reasonably well with metal scavenging residence times based on the distribution of elements in the ocean with the exception of Sc (Craig, 1974). The disagreement in estimating the scavenging residence time of Sc as indicated in Table 7 is perhaps due to analytical error in the water column data.

6. Material fluxes

One of the important aspects of the PARFLUX experiments is to determine the material fluxes at various depth horizons of the water column. Before discussing this

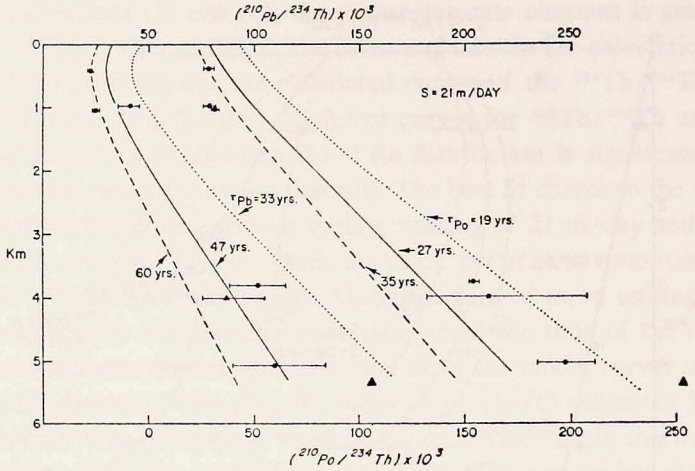

Figure 9. Comparison of the calculated ^{210}Pb/^{234}Th, and ^{210}Po/^{234}Th curves with the data. See text for discussion.

we first must know the trapping efficiencies of each trap for settling particles. This is especially important because the traps used in these experiments were originally designed to collect large particles, yet they clearly also collect significant quantities of fine particles. The trapping efficiency is hard to estimate based on the available hydrodynamical data. An alternative estimate can be made based on the reactive radionuclide flux data listed in Table 9.

(1) ^{230}Th: Consideration of the vertical material balance of ^{230}Th in the water column gives information on the trapping efficiency for particles (Spencer *et al.*, 1978). Since the ^{230}Th concentration in sea water is negligible compared to that of ^{234}U, we can assume that the production rate of ^{230}Th by the decay of ^{234}U in the water column above the trap is equal to the vertical flux of ^{230}Th at the depth of the trap deployed. Thus, by comparing the measured ^{230}Th flux with the calculated pro-

Table 8. Residence times of scavenging elements.

	$\psi_{Me}C_{Me}$ (μg kg^{-1} yr^{-1})	C_{Me} (μg kg^{-1})	τ_ψ (Years)	Other Estimates (Years)
Mn	1.5×10^{-3}	0.03	20	54 (Pacific)
		Bender *et al.*, 1977		Weiss, 1977
Fe	1.3×10^{-2}	1	77	
Cu	2.6×10^{-4}	0.13	500	1100 (Pacific)
		Moore, 1978		Boyle *et al.*, 1977
		Bender and Gagner, 1976		
Sc	2.6×10^{-6}	6×10^{-4}	230	2500 (Pacific)
				Craig, 1974

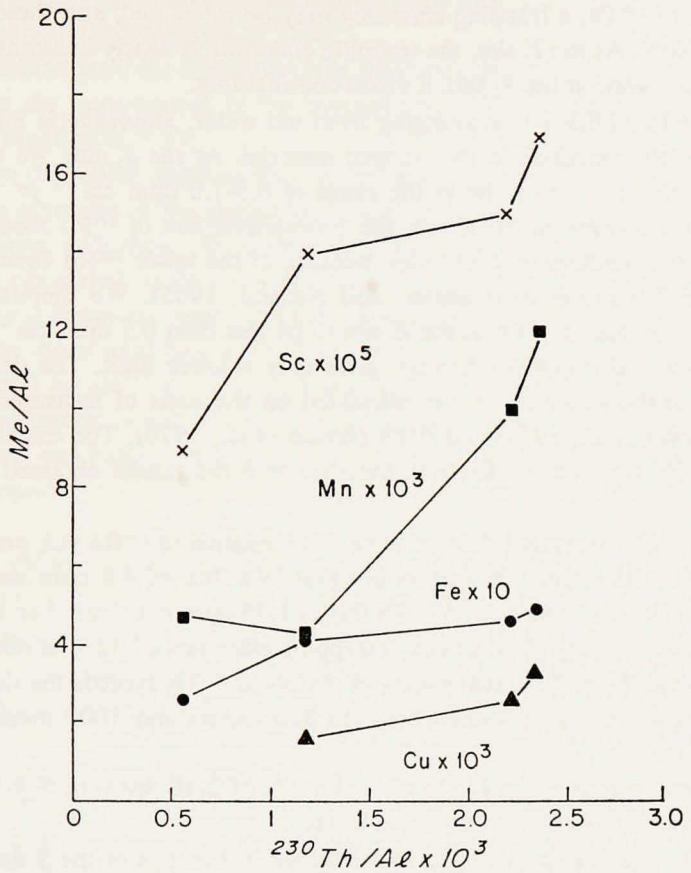

Figure 10. Plot of Metal/Al (g/g) versus ^{230}Th/Al (dpm/g) for Sc, Mn, Fe, and Cu.

Table 9. Radionuclide fluxes at the PARFLUX sites (dpm/cm^2/yr).

	PARFLUX *E* site				PARFLUX *S* site	
	398 m	988 m	3755 m	5086 m	1000 m	4000 m
^{234}Th	8.16	5.78	6.37	6.17	2.53	4.26
^{228}Th excess ($\times 10^{-2}$)	2.48	1.97	2.25	3.11	1.69	3.88
^{230}Th excess ($\times 10^{-3}$)	0.72	2.00	7.62	8.81	0.51	6.01
^{232}Th ($\times 10^{-3}$)	0.70	1.11	1.94	2.17	0.16	0.60
^{210}Pb	0.18	0.24	0.65	0.68	0.06	0.37
^{210}Po	0.23	0.17	0.98	1.21	0.08	0.68
^{226}Ra excess ($\times 10^{-3}$)	6.27	3.80	2.94	1.99	1.89	5.25
^{238}U ($\times 10^{-3}$)	2.27	1.61	1.61	1.99	0.64	1.00
^{231}Pa ($\times 10^{-3}$)	—	0.13	0.45	0.45	—	—

duction rate of ^{230}Th, a trapping efficiency may be calculated, and these results are given in Table 9. At the *E* site, the trapping efficiency is nearly constant with depth at about 75%, while at the S_2 site, it varies considerably.

(2) ^{210}Pb: In addition to scavenging from sea water, atmospheric input contributes to the ^{210}Pb contained in the trapped material. At the S_2 site, we estimate the atmospheric flux of ^{210}Pb to be in the range of 0.5-1.0 dpm cm^{-2} yr^{-1} (Turekian *et al.*, 1977). However, at the *E* site, the atmospheric flux of ^{210}Pb should be lower than that in the northern mid-latitudes, because of the lower ^{222}Rn concentration in the Equatorial atmosphere (Lambert and Nezami, 1965). We therefore estimate the atmospheric flux of ^{210}Pb at the *E* site to be less than 0.5 dpm cm^{-2} yr^{-1}, and thus the calculated trapping efficiency gives only a lower limit. The degree of disequilibrium in the water column is calculated on the basis of measured profiles of ^{226}Ra (Broecker *et al.*, 1976) and ^{210}Pb (Bacon *et al.*, 1976). The calculated results based on ^{210}Pb are given in Table 9, together with the results obtained from ^{230}Th fluxes.

(3) ^{228}Th: The measured deficiency of ^{228}Th relative to ^{228}Ra (Li, personal communication) in the upper 300 meters is equal to a flux of 4.8 dpm cm^{-2} yr^{-1} at both *E* and *S* sites. The measured ^{228}Th flux is 1.55 dpm cm^{-2} yr^{-1} at 1000 meters at the *S* site. Comparing these values, a trapping efficiency of 32% is obtained. This may be an upper limit if the scavenging of dissolved ^{228}Th exceeds the decay of particulate ^{228}Th in the water column between 300 meters and 1000 meters (Li, personal communication).

The 398 meter trap at the *E* site yielded a flux of 2.48 dpm cm^{-2} yr^{-1} of ^{228}Th, which corresponds to a 62% trapping efficiency.

(4) ^{234}Th: The removal of ^{234}Th in the upper 300 meters of the *S* site, estimated by assuming the same removal rate constant as for ^{228}Th, is 10.6 dpm cm^{-2} yr^{-1} (Spencer *et al.*, 1978). The measured flux of ^{234}Th at 1000 meters is 2.53 dpm cm^{-2} yr^{-1}. Assuming equilibrium between scavenging and decay in the water column between 300 meters and 1000 meters, then comparison of the above values yields 24% for the trapping efficiency.

Table 10. Estimates of trapping efficiencies for particles based on various radionuclides.

		Nuclides			
		^{230}Th	^{210}Pb	^{228}Th	^{234}Th
PARFLUX E —	398 m	70	> 49	62	77
	988 m	78	> 70	—	—
	3755 m	78	> 98	—	—
	5086 m	67	> 74	—	—
PARFLUX S_2 —	976 m	20	18-7	32	24
	3964 m	58	51-30	—	—

At the *E* site, the 398 meter trap collected 8.16 dpm cm^{-2} yr^{-1} of ^{234}Th, corresponding to a trapping efficiency of 77%.

Of the nuclides used for estimating trap efficiency the ^{230}Th estimate is to be preferred, given the uncertainties in the atmospheric ^{210}Pb contribution and the complex source function of ^{228}Th.

The above discussion suggests that the available radionuclide data are consistent in providing estimates of the particulate trapping efficiency. After correction of the measured fluxes with these efficiencies, the fluxes of each component and the total material, as calculated on the basis of excess ^{230}Th, and are given in Table 11. The calculated total fluxes are nearly constant with depth within a standard deviation of ± 15%. The mean total flux is 2500 μg cm^{-2} yr^{-1} at the *E* site, which is about twice the 1340 μg cm^{-2} yr^{-1} at the *S* site. Interestingly, the suspended particulate matter concentration is only about 4 $\mu g/kg$ in the mid-water column at the *E* site, which is about one-half of the 9 $\mu g/kg$ at the *S* site (Spencer *et al.*, 1978). It is clear that the trapped material is not simply related to the membrane-filtered particulate materials.

Table 11 shows a systematic increase of the clay particle flux with depth. A simple linear extrapolation from these data to the surface yields a surface deposition flux of 66 μg cm^{-2} yr^{-1} at the *S* site corresponding to an atmospheric Al flux of 5.5 μg cm^{-2} yr^{-1}. Spencer *et al.* (1978) estimated a value of 5 μg cm^{-2} yr^{-1} over the North Atlantic based on atmospheric particulate concentrations and air settling velocities (Buat-Menard and Chesselet, 1977). Considering the uncertainty of the estimates, this agreement is remarkable.

At the *E* site, the extrapolated surface clay particle flux is 250 μg cm^{-2} yr^{-1} corresponding to a primary Al flux of 20 μg cm^{-2} y^{-1}. The higher atmospheric dust flux at the *E* site is to be expected from the difference in wind patterns at these two sites (Trade Winds vs. Westerlies), and agrees with the observation of particulate Al concentration in the surface waters reported by Krishnaswami and Sarin (1976a).

7. The increasing alumino-silicate flux

In spite of the attractiveness of the vertical model presented earlier, it fails to explain a most important experimental observation: the increase of the alumino-silicate flux with depth at both the S_2 and *E* sites. There are two possible explanations for this observed increase: that it is an experimental artifact produced by overtrapping of fine clay particles, or that there is an additional source of material extrinsic to the vertical flux.

Since the chemical composition of the alumino-silicate material is invariant with depth at the *E* site (Figs. 2 and 3), it implies that the trapped material at all depths must have originated from a uniform source.

The vertical flux of Al (F_{Al}) at any depth is given by:

$$F_{Al} = \bar{S}\chi_{Al} - W\chi_{Al} - D\frac{\partial_{\chi Al}}{\partial Z} \tag{12}$$

where $\bar{S}$ is mean settling velocity (cm/sec), D is eddy diffusion coefficient (cm²/sec) and Z is the water depth.

At steady state, the flux of Al (F_{Al}) must be constant with depth, i.e., $dF_{Al}/dZ = 0$. Therefore, neglecting diffusion and advection it follows,

$$\chi_{Al}\frac{\partial \bar{S}}{\partial Z} = \bar{S}\frac{\partial_{\chi Al}}{\partial Z} \tag{13}$$

Thus, any decrease of the mean settling velocity of Al by disintegration and dissolution of large biogenic particles must be followed by an increase in total concentration of particulate Al with increased fine clay particles. This is, in fact, probably occurring because the fluxes of all biogenic particles which control clay particles are decreasing with depth. Therefore, if Al containing fine particles are trapped in a manner proportional to concentration at the depth of the trap deployed, the measured Al flux would be expected to increase with depth.

According to equation (13), the decrease of the mean settling velocity of Al bearing particles with depth by disintegration and dissolution of biogenic large particles implies that water diffusion and advection become increasingly important and reduction of turbulence within the trap cone will increase the fine particle flux. However, this contribution must be very small in the normal vertical diffusion and advection regime (D = 1 cm²/sec and w = $\sim 1 \times 10^{-5}$ cm/sec; Craig, 1969), even if complete stagnation of water occurred within the collection cone of the moored trap. In order to explain possible overtrapping of Al, a focussed aggregation process of fine clay particles would be required. This is possibly biological, for example due to attraction of filter-feeding zooplankton around the trap. Sticking of fine clay particles on the wall of the PVC traps may also need to be considered, and such a phenomenon has been observed by Hodge *et al.* (1979). This may be followed by aggregation with large particles along the slope of the trap.

If the measured Al flux is not significantly modified by experimental artifacts, then the increase with depth requires a significant source within the water column

Table 11. Material fluxes corrected by excess ^{230}Th based on trapping efficiency (μg cm^{-2} yr^{-1}).

	PARFLUX *E* site				PARFLUX S_2 site	
	398 m	988 m	3755 m	5086 m	1000 m	4000 m
Total mass	2700	2064	2513	2701	1400	1276
Clay	327	433	942	1240	132	330
Carbonate	1445	1054	1001	1113	918	799
Opal	300	206	134	119	91	0
Organic matter	629	369	155	230	255	147

in addition to the primary atmospheric supply. Although resuspension of fine particles from the bottom has been observed by many workers (see Brewer *et al.*, 1976), it seems unlikely that this would affect the Al flux throughout the 5000 meter water column. The only remaining source is the advective horizontal transport of fine particles from near the continental margins.

By taking the horizontal transport along the X direction witht velocity U, the distribution of particulate Al ($_{Al}$) is given by:

$$U\frac{\partial \chi_{Al}}{\partial X} = D\frac{\partial^2 \chi_{Al}}{\partial Z^2} - \bar{S}\frac{\partial \chi_{Al}}{\partial Z} - k\chi_{Al} \tag{14}$$

where k is a removal rate constant of particulate Al assuming a first-order process and representing aggregation of fine particles and accelerated sinking. The integrated flux of Al as given in Table 10, shows an almost linear increase with depth, so that

$$F_{Al}(Z) = F_{Al}{}^{a} + bZ = F_{Al}{}^{a} + \int_{0}^{Z} k\chi_{Al}\, dZ \tag{15}$$

where b is a constant obtained from the slope of an increasing Al flux and $F_{Al}{}^{a}$ is an atmospheric flux of Al.

Differentiating equation (15), we obtain,

$$b = k\chi_{Al} \tag{16}$$

which requires $\partial\chi_{Al}/\partial Z = 0$, if k is constant with depth. Therefore, Equation (14) can be simplified to

$$U\frac{\partial \chi_{Al}}{\partial X} = -k\chi_{Al} \tag{17}$$

The solution of equation (17) is given by

$$\chi_{Al} = \chi_{Al}{}^{o} \exp\left(-\frac{k}{U} \cdot X\right) \tag{18}$$

or

$$F_{Al} = F_{Al}{}^{o} \exp\left(-\frac{k}{U} \cdot X\right) \tag{19}$$

where $\chi_{Al}{}^{o}$ and $F_{Al}{}^{o}$ are the particulate Al concentration and the particulate Al flux respectively, in the source regions at the horizontal boundary ($X = 0$).

Equation (19) implies measurable gradients in the particulate alumino-silicate concentrations away from a continental slope boundary. Substantial evidence for this has been reported by many workers. Eittrem *et al.* (1976) have presented maps of the turbidity distribution in the Atlantic Ocean. They observed variations in turbidity of a factor of three or more between basin margins and centers. The most turbid water was associated with the western boundary bottom currents, as was reported by Brewer *et al.* (1976), and the southern extension of this flow may have

affected the *E* site. Recently Biscaye and Eittrem (1977) have reported data showing a turbidity maximum close to the PARFLUX S_2 site. Armi (1978) has recently emphasized the importance of boundary mixing, and has presented nephelometer data showing horizontal transport of fine particulates away from a continental boundary. However, although there is compelling evidence for the importance of horizontal particulate transport, considerable difficulties exist in directly incorporating these observations into the experiment reported here. The conversion of turbidity measurements or water bottle sampled particulates, into flux estimates is not easy (Bishop *et al.*, 1977). Moreover, there are geochemical problems in reconciling the unique radioisotopic signal presented by the trapped material with observations characteristic of the surficial layer of marine sediments.

Both Bacon *et al.* (1976) and Brewer and Hao (1979) have emphasized the importance of horizontal boundaries in controlling scavenging residence times; thus the settling velocities and scavenging residence times derived here from the application of a simple vertical model must be regarded as model constructs, resulting of necessity from the availability of a purely one-dimensional data set. The placement of sediment traps in line away from a continental boundary would be an important experiment in resolving the problems raised here.

Acknowledgments. We would like to thank Dr. S. Honjo, who conducted the PARFLUX program and cooperated throughout the study. We are grateful to K. K. Turekian, S. Honjo and M. P. Bacon for stimulating discussions, and Y. H. Li for providing his unpublished GEOSECS ^{228}Ra-^{228}Th data for calculations. Critical comments were supplied by P. Buat-Menard, R. Chesselet and M. L. Bender. Dr. Krishnaswami at Yale University greatly contributed in the early stage of the study, especially in radiochemical analysis of samples obtained at the S_2 site. We wish to acknowledge the help of C. L. Smith, J. Connell, P. Clay and P. O'Malley in work at sea and in mooring and trap deployment. The assistance of Captains E. Hiller, D. Casiles, P. Howland, the officers and crew of the R.V. *Knorr,* R.V. *Oceanus* and R.V. *Atlantis II* are gratefully acknowledged. Support for this work was provided by the National Science Foundation Grant OCE 77-27004 and Department of Energy, Contract EY-76-S-02-3566 to Woods Hole Oceanographic Institution and from the National Science Foundation under Grant OCE 76-20239 to Yale University, (K. K. Turekian, Principal Investigator). This is Woods Hole Oceanographic Institution Contribution No. 4451.

REFERENCES

Armi, L. 1978. Some evidence for boundary mixing in the deep ocean. J. Geophys. Res., *83,* 1971–1979.

Bacon, M. P., D. W. Spencer and P. G. Brewer. 1976. ^{210}Pb/^{226}Ra and ^{210}Po/^{210}Pb disequilibria in seawater and suspended particulate matter. Earth Planet. Sci. Lett., *32,* 277–296.

Bender, M. L. and C. L. Gagner. 1976. Dissolved copper, nickel and cadmium in the Sargasso Sea. J. Mar. Res., *34,* 327–339.

Bender, M. L., G. P. Klinkhammer and D. W. Spencer. 1977. Manganese in seawater and the marine manganese balance. Deep-Sea Res., *24,* 799–812.

Berger, W. H. and A. Soutar. 1967. Planktonic foraminifera: field experiment on production rate. Science, *156,* 1495–1497.

Biscaye, P. E. and S. L. Eittrem. 1977. Suspended particulate loads and transports in the nepheloid layer of the abyssal Atlantic Ocean. Mar. Geol., *23,* 155–172.

Bishop, J. K. B., J. M. Edmond, D. R. Ketten, M. P. Bacon and W. B. Silker. 1977. The chemistry, biology and vertical flux of particulate matter from the upper 400 m of the equatorial Atlantic Ocean. Deep-Sea Res., *24,* 511–548.

Boyle, E. A., F. R. Sclater and J. M. Edmond. 1977. The distribution of dissolved copper in the Pacific. Earth Planet. Sci. Lett., *37,* 38–54.

Brewer, P. G. 1975. Minor elements in seawater, *in* Chemical Oceanography, Vol. 1. Second Edition, J. P. Riley and G. Skirrow, eds., Academic Press, London, 606 pp.

Brewer, P. G., D. W. Spencer, P. E. Biscaye, A. Hanley, P. L. Sachs, C. L. Smith, S. Kadar and J. Fredericks. 1976. The distribution of particulate matter in the Atlantic Ocean. Earth Planet. Sci. Lett., *32,* 393–402.

Brewer, P. G. and W. M. Hao. 1979. Oceanic elemental scavenging, *in* Chemical Modelling in Aqueous Systems, E. A. Jenne, ed., ACS Symposium Series, 93. American Chemical Society, Washington, D.C., 914 pp.

Broecker, W. S., J. Goddard and J. L. Sarmiento. 1976. The distribution of ^{226}Ra in the Atlantic Ocean. Earth Planet. Sci. Lett., *32,* 220–235.

Buat-Menard, P. and R. Chesselet. 1977. Marine aerosols control on deep ocean heavy metals particulate chemistry. Proc. Ninth Int. Conf. on Atmospheric Aerosols, Condensation and Ice Nuclei; Galway, Ireland, 21-27 September 1977, Pergamon Press.

—— 1979. Variable influence of the atmospheric flux on the trace metal chemistry of oceanic suspended matter. Earth Planet. Sci. Lett., *42,* 399–411.

Chan, L. H., D. Drummond, J. M. Edmond and B. Grant. 1977. On the barium data from the Atlantic GEOSECS expedition. Deep-Sea Res., *24,* 613–649.

Craig, H. 1969. Abyssal carbon and radiocarbon in the Pacific. J. Geophys. Res. *74,* 5491–5506.

—— 1974. A scavenging model for trace elements in the deep sea. Earth Planet. Sci. Lett., *23,* 149–159.

Dehairs, F., R. Chesselet and J. Jedwab. 1980. Discrete suspended particles of barite and the barium cycle in the open ocean. Earth Planet. Sci. Lett., in press.

Deuser, W. G. and E. H. Ross. 1980. Seasonal change in the flux of organic carbon to the deep Sargasso Sea. Nature, *283,* 364–365.

Eittrem, S., E. M. Thorndike and L. Sullivan. 1976. Turbidity distribution in the Atlantic Ocean. Deep-Sea Res., *23,* 1115–1127.

Gardner, W. D. 1980a. Sediment trap dynamics and calibration: a laboratory evaluation. J. Mar. Res., *38,* 17–39.

—— 1980b. Field assessment of sediment traps. J. Mar. Res., *38,* 41–52.

Hargrave, B. T. and N. M. Burns. 1979. Assessment of sediment trap collection efficiency. Limnol. Oceanogr., *24,* 1124–1136.

Hinga, K. R., J. McN. Sieberth and G. R. Heath. 1979. The supply and use of organic material at the deep-sea floor. J. Mar. Res., *37,* 557–579.

Hodge, V. F., M. Koide and E. D. Goldberg. 1979. Particulate uranium, plutonium and polonium in the biogeochemistry of the coastal zone. Nature, *277,* 206–209.

Honjo, S. 1978. Sedimentation of material in the Sargasso Sea at a 5367 m deep station. J. Mar. Res., *36,* 469–492.

—— 1980. Material fluxes and modes of sedimentation in the mesopelagic and bathypelagic zones. J. Mar. Res., *38,* 53–97.

Honjo, S. and J. F. Connell. 1979. Construction of PARFLUX Mark II sediment trap; engineering report. Woods Hole Oceanographic Institution Technical Report WHOI-79-80. 49 pp.

Knauer, G. A., J. H. Martin and K. W. Bruland. 1979. Fluxes of particulate carbon, nitrogen and phosphorus in the upper water column of the northeast Pacific. Deep-Sea Res., *26,* 97–108.

Krishnaswami, S. and M. M. Sarin. 1976a. Atlantic surface particulates: composition, settling rates and dissolution in the deep sea. Earth Planet. Sci. Lett., *32,* 430–441.

—— 1976b. Procedure for the simultaneous determination of Th, Pu and Ra isotopes, ^{210}Pb, ^{55}Fe, ^{32}Si, ^{14}C in marine suspended phases. Anal. Chim. Acta, *83,* 143–156.

Lambert, G. and M. Nezami. 1965. Importance des retombees seches dans le bilan du plomb 210. Ann. Geophys., *21,* 245–251.

Moore, R. M. 1978. The distribution of dissolved copper in the eastern Atlantic Ocean. Earth Planet. Sci. Lett., *41,* 461–468.

Spencer, D. W., P. G. Brewer, A. P. Fleer, S. Honjo, S. Krishnaswami and Y. Nozaki. 1978. Chemical fluxes from a sediment trap experiment in the deep Sargasso Sea. J. Mar. Res., *36,* 493–523.

Taylor, S. R. 1964. Abundance of chemical elements in the continental crust: A new table. Geochim. Cosmochim. Acta, *28,* 1273–1286.

Trier, R. M., W. S. Broecker and H. W. Feely. 1972. ^{228}Ra profile at the second GEOSECS intercalibration station 1970 in the North Atlantic. Earth Planet. Sci. Lett., *16,* 141–145.

Turekian, K. K. 1965. Some aspects of the geochemistry of marine sediments, *in* Chemical Oceanography, Vol. 2, First Edition. J. P. Riley and G. Skirrow, eds., Academic Press, London, 508 pp.

Turekian, K. K., D. P. Kharkar and J. Thomson. 1973. Uranium and thorium decay series nuclide abundances in marine plankton. Final report to Advanced Research Projects Agency, ARPA.

Turekian, K. K., Y. Nozaki and L. K. Benninger. 1977. Geochemistry of atmospheric radon and radon products. Ann. Rev. Earth Planet. Sci., *5,* 227–255.

Turekian, K. K. and Y. Nozaki. 1979. ^{210}Po and ^{210}Pb in the eastern South Pacific: the role of upwelling on their distributions in the water column. Earth Planet. Sci. Lett. (in press).

Weiss, R. F. 1977. Hydrothermal manganese in the deep sea: scavenging residence times and manganese/helium-3 relationships. Earth Planet. Sci. Lett., *37,* 257–262.

Wiebe, P. H., S. H. Boyd and C. Winget. 1976. Particulate matter sinking to the deep-sea floor at 2000 m in the Tongue of the Ocean, Bahamas, with a description of a new sedimentation trap. J. Mar. Res., *34,* 341–354.

Wong, G. T. F., P. G. Brewer and D. W. Spencer. 1976. The distribution of particulate iodine in the Atlantic Ocean. Earth Planet. Sci. Lett., *32,* 441–450.

Received: *5 January, 1980*; revised: *1 July, 1980.*